Effects of superheated flash-boiling atomisation on spray carbon capture performance

Louis F. Dacanay*[1], Kevin Wan[2], Julien Manin[2], Ian A. Gass[1], Alain Ledoux[3], Lionel Estel[3], Cyril Crua[1]
[1] Advanced Engineering Centre, University of Brighton, Brighton, UK
[2] Combustion Research Facility, Sandia National Laboratories, Livermore, CA 94550
[3] Normandie Université, INSA Rouen, LSPC, FR-76000 Rouen, France
*Corresponding author: e.dacanay2@uni.brighton.ac.uk

Abstract
In light of recent climate and environmental goals, there is an urgent need for the development of efficient mitigation technologies such as carbon capture. While spray-based carbon capture systems can offer high CO_2 absorption rates compared to packed columns, their optimisation requires a fine control on spray homogeneity and droplet properties (e.g. size and relative velocity). More specifically, denser mono-disperse sprays with micron scale droplets have been found to increase the rate of CO_2 absorption. One approach that has not previously been investigated is to control the solvent spray properties through flash boiling atomisation to consistently produce fine and homogenous droplets. To address this gap, we present optical measurements comparing the performance of solvents atomised with and without flash boiling. Diffuse-back illumination extinction imaging was used for temporal characterisation of spray morphology. We tested a 20:80 (% w/w) blend of triethanolamine and methanol under four temperature conditions to vary the amount of superheat. Absorption capacities and CO_2 concentration removal are reported for each tested condition, showing significant improvements at the higher temperature conditions.

1. Introduction

Recent greenhouse gas projections have indicated that without a change in climate policy or technological reforms, achieving climate goals of net zero CO_2 by 2050 and limiting global warming to 1.5-2°C this century will be a challenging task [1]. With this, major governments have employed the use of CCS (carbon capture and storage) technologies within their nationwide strategies to mitigate CO_2 emissions [2,3]. Post combustion gas purification via liquid solvent absorption, being the most mature method for removing anthropogenic emissions, has been listed as a key technology in achieving global climate goals [4]. The conventional gas absorption process utilises two closed structures: An absorber column where the liquid solvent is introduced top-side against the counterflowing flue gas (at temperatures of 313-323 K), and a stripper column where the rich solvent is heated to release the captured CO_2 (at temperatures of 403-413 K), after which the clean solvent is cycled back to the absorber for reuse [5,6]. These columns are typically used for stationary heavy emitting sources such as cement/steel production and fossil-fuel powered energy plants [7]. Although, they can also be used for cleaning streams containing lean amounts of CO_2 using aqueous amines such as MEA (monoethanolamine), which is the current industry standard due to its low cost and high chemical reactivity [8-10]. CO_2 absorption is achieved using absorption contactors (e.g. packed columns, trays, and sprays) within the absorber column that aim to increase the surface area contact between the liquid chemical absorbent and flue gas [11]. Sprays have been found to perform better than packed columns and trays because of increased volumetric mass transfer from the larger gas-liquid interfacial area droplets provide [12]. Furthermore, sprays offer minimal pressure drop and have low maintenance costs due to their simple infrastructure [13]. Liquid droplet size has been reported to correlate directly with CO_2 absorption performance. Smaller droplets (Sauter mean diameter < 50 µm at lab scale) increased the absorption rate and overall CO_2 removal; This is due to the increased overall liquid surface area and reduced diffusion time for the gas molecules across each droplet [14-16]. A polydisperse spray lowers the overall average absorption capacity due to its large size distribution and thus irregular CO_2 diffusion time per droplet. Therefore, homogeneous mono dispersed sprays are favoured as they offer more control over absorption rate, larger absorption capacities, and decrease pressure drop more effectively given low gas flow rates [14,17]. Currently in the literature, a universal optimal droplet size has not been defined for spray capture as it is dependent on a variety of operational conditions and absorber properties (e.g., gas flow rate, injection pressure, liquid flow rate). While a smaller droplet diameter extends absorption capabilities, the droplets are more susceptible to fly back and collisions with the column wall from the high velocity counter-flowing gas, resulting in solvent losses [18]. Faster droplet velocities caused by higher injection pressures may reduce the CO_2 capture efficiency due to shorter residence time, although this can be balanced out with faster reacting solvents [19]. Regardless, there is a consensus that indicates operating with a smaller droplet regime yields a higher capture performance. Adjustment of the injector type remains the primary method of modifying liquid solvent atomisation characteristics for CO_2 spray capture. Some examples include the use of a full cone nozzle, multi-nozzle plate,

ultrasonic nozzle, spiral tip and swirl chamber nozzle, pressure swirl atomiser, and dual nozzle impinging atomiser [14, 20-24]. None have explored adjusting injector-chamber conditions to achieve liquid break up via the flash boiling mechanism, which is commonly observed in modern direct injection engines [25, 26]. Flash boiling atomisation occurs when a liquid is brought into a metastable superheated state. Specifically, when the environment pressure the liquid is injected into is lower than the saturation pressure of the liquid itself [27]. This form of breakup has been reported to produce consistently fine droplet (SMD's < 50 μm) and high droplet number densities (up to 18×10^3 mm^3) at a liquid temperature range of 293-383 K and low injection pressures [28]. Furthermore, with a greater degree of superheat (amount at which liquid is heated past its boiling temperature) a narrowing of the spray plume angle is observed [29], thus reducing the penetration length of the spray. Although these properties are particularly attractive for spray CO_2 absorption applications, it appears that no previous research has been published on this particular approach. To address this gap we provide quantitative results on the overall CO_2 absorption when adopting the flash boiling mechanism for liquid solvent atomisation. The objective was to examine the effects of varying superheating degree of the solvent on capture performance using a blend of triethanolamine (tertiary class of amine solvent) and methanol. Methanol was chosen to reduce the specific heat of the solvent, in order to reduce the energy required for thermal regeneration compared to aqueous blends [30]. Absorption capacities of the solvent blend over the range of nozzle-chamber temperature conditions and subsequent CO_2 concentration drops are reported.

2. Material and methods

2.1 Apparatus and approach

Figure 1 displays a schematic of the experimental setup consisting of a constant volume spray vessel, high-speed camera, IR camera, and an LED light source. A single-hole injector (BOSCH HDEV-1-1HF) was used for solvent blend injection. Diffuse backlit imaging (DBI) was implemented using the high-speed camera (Phantom v2512) positioned at the eastern port of the chamber perpendicular to the injection direction, and 520 nm LED source with diffuser directly opposite at the western port. During the injection period, DBI images of the spray morphology was captured to verify the occurrence of flash boiling. The IR camera (FLIR X6900sc) operating at 1 kHz was fitted with a 4.26 μm IR bandpass filter (Edmund Optics, 84-073) and placed at the southern port facing directly towards the injector for IR imaging of the injector region. The spray vessel used sapphire windows at each of the open ports (east, west, and south) for optical access to the vessel's interior. The cartridge heaters and spray vessel were heated using a PID temperature control system.

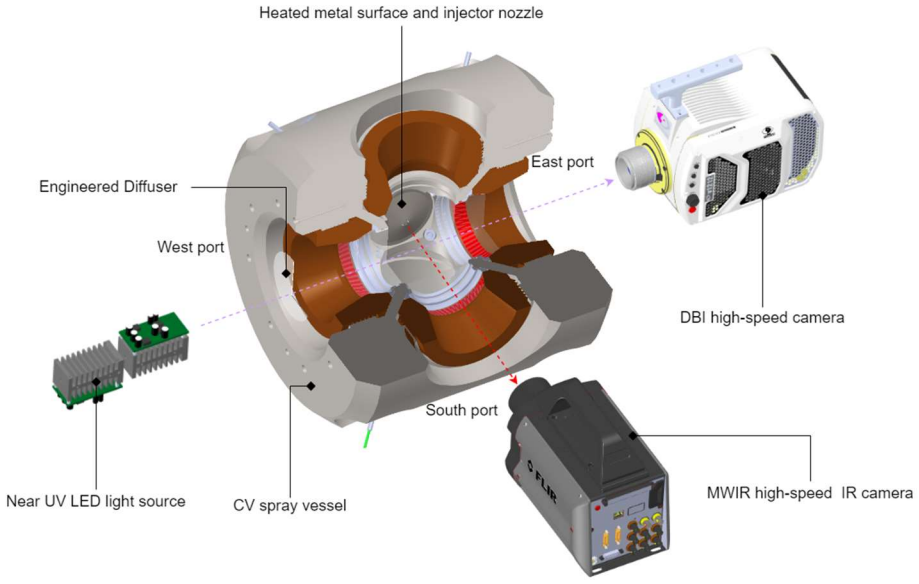

Figure 1. Schematic of experimental setup displaying position of near UV LED, IR camera, and high-speed camera relative to the constant volume spray vessel and injector. The red arrow represents the injection direction as well as the direction of IR radiation from the heated injector nozzle.

Figure 2 displays a sectioned view of the spray vessel chamber and optical setup. The injector itself is fixed in a metallic flange case that was heated using six cartridge heaters which surround the injector tip. Inlet and exhaust valves used for CO_2 filling and purging are mounted at the corners of the spray vessel which is the top and bottom

left regions in Figure 2. The CO_2 within the chamber was not stationary throughout the experiment as a fan operating at approximately 1000 rpm was used to reduce thermal stratification.

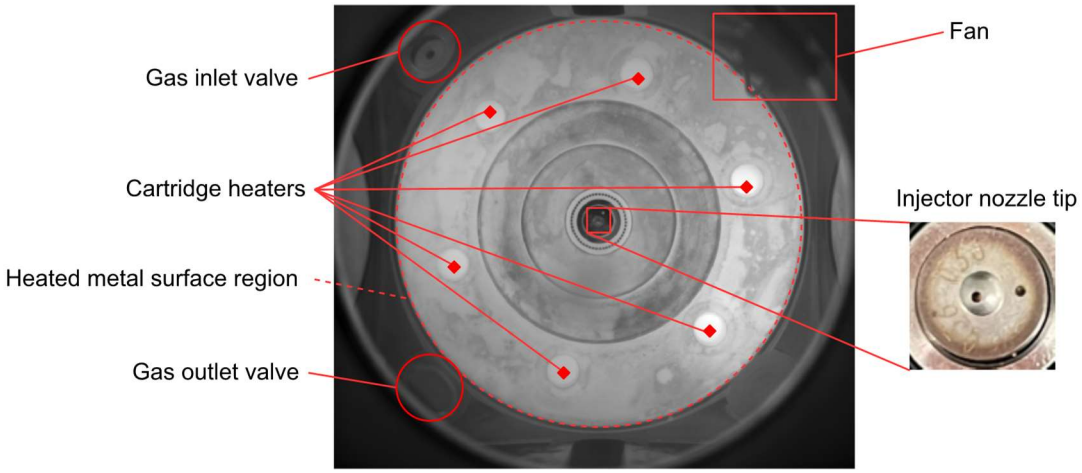

Figure 3. Infrared view of the chamber from IR camera with annotations for the key components within view. A (non-IR) snippet of the injector nozzle tip is also included.

The rationale behind taking an IR optical approach was to gather quantitative CO_2 gas concentrations at specific regions of the chamber during and after the injection process, which can then be used to quantify the absorption rate. This approach was also used for confirming the spray structure and confirm the degree of flash boiling. Finally, optical imaging methods offer the capability of mapping out spatial and temporal evolution of gas concentrations within the chamber pre, post, and during solvent injection. The IR images captured for this investigation were within the MWIR (mid-wave infrared) spectral band, specifically at the 4.2 μm wavelength. IR videos were captured when the vessel was filled with N_2 (reference), during the CO_2 filling process, injection period, and CO_2 purging process. Each test point consisted in a total of 8 injection videos, with each video having 4x solvent injections (hence a total of 32 injections). To quantify CO_2 concentrations from the IR images, correlations were made between image intensities and CO_2 gas densities. Figure 4 displays a simplified diagram for the IR radiation transfer occurring from heated injector nozzle and metal surface towards the thermal sensor within the IR camera. Some components within the experiment emitted and/or absorbed IR radiation within the spectral band, one such being the CO_2 gas which simultaneously emitted and absorbed heavily at the observed wavelength band. Therefore, the absorption and emission of each individual component within the experiment had to be considered in order to compute the CO_2 concentration from the recorded IR intensities.

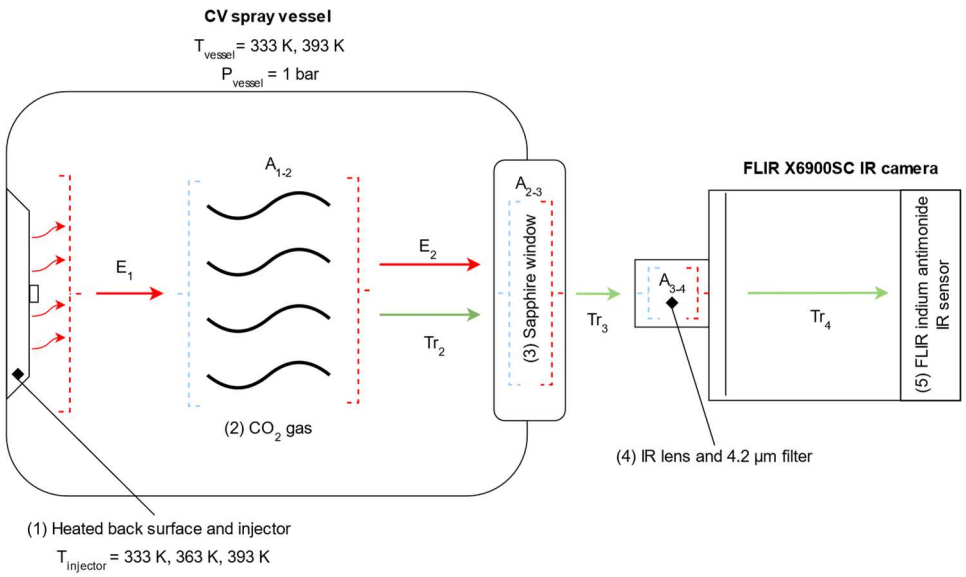

Figure 2. Heat transfer diagram starting from the heated metal surface/injector towards the FLIR IR camera and computer system. Each absorbing/emitting component in the rig is labelled (1-5). Labels "A" indicate points where IR absorption take place (e.g. $A_{1\text{-}2}$ indicates absorption of incident radiation coming from the injector by the CO_2 gas). Labels "E" indicate IR emission points (e.g. E_2 indicates separate emission from the heated CO_2 gas). Labels "Tr" indicate transmitted IR radiation through the previous absorbing/emitting component (e.g. Tr_1 represents IR radiation which has passed through the CO_2 gas without getting absorbed).

2.2 Radiative heat transfer equation (RTE)

The radiative heat transfer equation describing the change of intensity (at a specific spectral range) with optical distance through a medium (in this case CO_2) that simultaneously absorbs and emits (neglecting scattering effects) is shown in Equation 1 [31]:

$$\frac{dI_\eta}{ds} = \kappa_\eta\left(I_{b\eta} - I_{\eta,0}\right) \tag{1}$$

where I_η is the transmitted (i.e. spatially attenuated) intensity [pixel counts], κ_η [m^{-1}] is the linear absorption coefficient of CO_2 , $I_{b\eta}$ [pixel counts] is the blackbody radiation of the CO_2, $I_{\eta,0}$ [pixel counts] is the incident intensity entering the CO_2 volume, and s [m] is the distance through the CO_2 or "path length". The product of κ_η and $I_{b\eta}$ refers to emission of the CO_2 and is proportional to the gas volume. The product of κ_η and $-I_{\eta,0}$ relates to the CO_2 absorption and is negative due to light intensity decreasing as it propagates through the gas volume. The linear absorption coefficient of CO_2 is calculated experimentally using the Lambert's attenuation law in equation 2 [32]:

$$\kappa_\eta = \frac{\ln\left(\frac{I_\eta}{I_{\eta,0}}\right)}{s} \tag{2}$$

2.2.1 Solution to the RTE and final modelling equation

For an isothermal gas layer with thickness s, the intensity transmitted through, whilst neglecting light scattering, can be obtained by integrating Equation 1 over path distance [31]:

$$I_\eta(s) = I_{\eta,0}e^{-\tau_\eta} + I_{b\eta}\left(1 - e^{-\tau_\eta}\right) \tag{3}$$

where

$$\tau_\eta = \rho_{CO_2} \int_0^s \kappa_{\rho\eta}\, ds \tag{4}$$

which is the dimensionless parameter "optical thickness" and $\kappa_{\rho\eta}$ is the mass absorption coefficient [m^2 kg^{-1}] calculated by dividing κ_η by CO_2 density. Note that $e^{-\tau_\eta}$ is equal to transmission, therefore 1 minus this value will give the absorption amount. When absorption amount is multiplied with the blackbody intensity of the CO_2 and given a positive sign, this results in the emission term. The entire term $(1 - e^{-\tau_\eta})$ is also the representation of CO_2

emissivity. Considering there is an absorption constant A relating absorption of external factors such as optics (sapphire windows, IR lens, and filter) as seen in Figure 2, Equation 3 is re-written as:

$$I_\eta(s) = AI_{\eta,0}e^{-\kappa_{\rho\eta}\, s\, \rho_{CO_2}} + AI_{b\eta}\left(1 - e^{-\kappa_{\rho\eta}\, s\, \rho_{CO_2}}\right) \quad (5)$$

In Equation 5 the constants A and $I_{b\eta}$ are experimentally unknown. Therefore, a simultaneous equation approach was taken to resolve this issue. Assuming a scenario where CO_2 concentration is known (e.g. 100% CO_2 environment), Equation 5 can be rearranged to solve for A as a function of $I_{b\eta}$:

$$A = \frac{I_{\eta,CO_2,100}}{\left(I_{\eta,0}e^{-\kappa_{\rho\eta}\, s\, \rho_{CO_2,100}} + I_{b\eta}\left(1-e^{-\kappa_{\rho\eta}\, s\, \rho_{CO_2,100}}\right)\right)} \quad (6)$$

where $I_{\eta,CO_2,100}$ [pixel counts] is the average intensity at 100% CO_2 concentration, and $\rho_{CO_2,100}$ [kg m^{-3}] is the theoretical density of CO_2 at the experimental temperature and pressure conditions. Because A is an experimental constant, Equation 6 is substituted back into Equation 5 giving:

$$I_\eta = I_{\eta,\,CO_2,100}\frac{I_{\eta,0}e^{-\kappa\rho\eta\, s\, \rho_{CO_2}} + I_{b\eta}\left(1-e^{-\kappa\rho\eta\, s\, \rho_{CO_2}}\right)}{I_{\eta,0}e^{-\kappa\rho\eta\, s\, \rho_{CO_2,100}} + I_{b\eta}\left(1-e^{-\kappa\rho\eta\, s\, \rho_{CO_2,100}}\right)} \quad (7)$$

where the only unknown remaining is $I_{b\eta}$ (blackbody radiation of the CO_2 in the spray vessel). $I_{b\eta}$ was computed iteratively until the output transmitted intensity (I_η) matched the experimental average intensity for a known CO_2 concentration (i.e. 100% CO_2, prior to the first solvent injection). As the gas was assumed to be under local thermodynamic equilibrium, $I_{b\eta}$ remains constant and does not change with ρ_{CO_2} (i.e. during the CO_2 absorption process). Equation 7 was used for building a model that was fitted to the experimental average intensities recorded from the high-speed IR videos. CO_2 densities at different time points, both pre- and post- solvent injection, could then be computed using the fitted model.

2.3 Experimental conditions and solvent blend

To simulate a degree of superheat for the flash boiling spray, four injector nozzle-chamber temperature conditions were tested which is shown in Table 1. The chemical solvent used for testing was a (20/80) wt% blend of triethanolamine ($C_6H_{15}NO_3$) and methanol (CH_3OH). Triethanolamine is a tertiary class type of amine and was selected for its high absorption capacity of 1, meaning 1 mol of amine is used in solution to absorb 1 mole of CO_2. This is contrast to primary/secondary amine types which require 2 moles of amine per mole of absorbed CO_2 [9,33]. The concentration of TEA was kept at 20 wt% as high amine concentrations are linked to increased thermal degradation of the solvent and system corrosion [34,35]. This was mixed with methanol to keep the solvent blend boiling point as low as possible and minimise the energy penalty when desorbing CO_2 for solvent regeneration. Furthermore, this methanol was used to decouple physical and chemical absorption reactions as will be explained in section 3.1. Table 2 summarises the properties of the solvent blend and its individual components.

Table 1. Nozzle-chamber temperature conditions, vessel, and injection pressures used for testing.

	Nozzle (solvent) temperature [K]	Spray vessel (CO_2) temperature [K]	Vessel pressure [atm]	Injection pressure [MPa]
Condition 1 (60TEA60)	333	333	1	0.6
Condition 2 (60TEA60)	363	333	1	0.6
Condition 3 (120TEA60)	393	333	1	0.6
Condition 4 (120TEA120)	393	393	1	0.6

Table 2. Solvent blend and component properties

	Triethanolamine (TEA)	Methanol	TEA and methanol blend
CAS number	102-71-6	67-56-1	-
Critical temperature [K]	782.14	513.4	567.15
Critical pressure [MPa]	4.32	8.22	7.44
Density [kg m^{-3}]	1124	786.06	786.64
Boiling point [K]	608.55	337.85	391.99

2.4 Image processing methodology

Figure 4 summarises the image processing methodology adopted to extract average pixel intensities from the IR images in preparation for fitting with the mathematical concentration model. The process begins with extracting dark image average counts during shutter closing and subtracting from the raw frames of each IR video. This is to correct any extra signal caused by the camera's own radiation. A small number of small 'hot' pixel clusters with abnormally high signal counts were corrected by thresholding those clusters and replacing them with the average of neighbouring pixels. Background radiation and hot pixel corrected frames are then masked. The region of interest (ROI) chosen for the mask was located at the upper left high emissivity region of the chamber beneath a cartridge heater (highlighted by red box in Figure 4). This area was chosen as it was less sensitive to gas stratification due to it being more elevated and nearer the fan (more homogenous gas distribution). Additionally, no window fouling could occur in this area, ensuring optical clarity. As the injector orifice was angled downwards, solvent deposits as a result of injection were observed on the bottom half of the sapphire window, but those did not affect the IR signal. Mean pixel intensities were then taken from the masked frames within the ROI at the beginning of each injection video. Averages at the beginning of the video were taken because when the solvent was injected, the chamber cooled down and decreased pixel intensity which can mislead calculations of CO_2 concentrations. The gas heats back up and thermally stabilises between each injection video to the temperature of the vessel, so the beginning of each injection video represents a period where the CO_2 is at local thermodynamic equilibrium. Equation 7 was then used to create a model for I_η and fitting with the mean pixel intensities from the image processing. This fitting process starts with finding $I_{b\eta}$ through the method described in section 2.2.1, which leaves ρ_{CO_2} as the only unknown in Equation 6. The model is fitted over all experimental mean pixel intensities calculated from the image processing (8 injection videos) using the statistical least squares regression method.

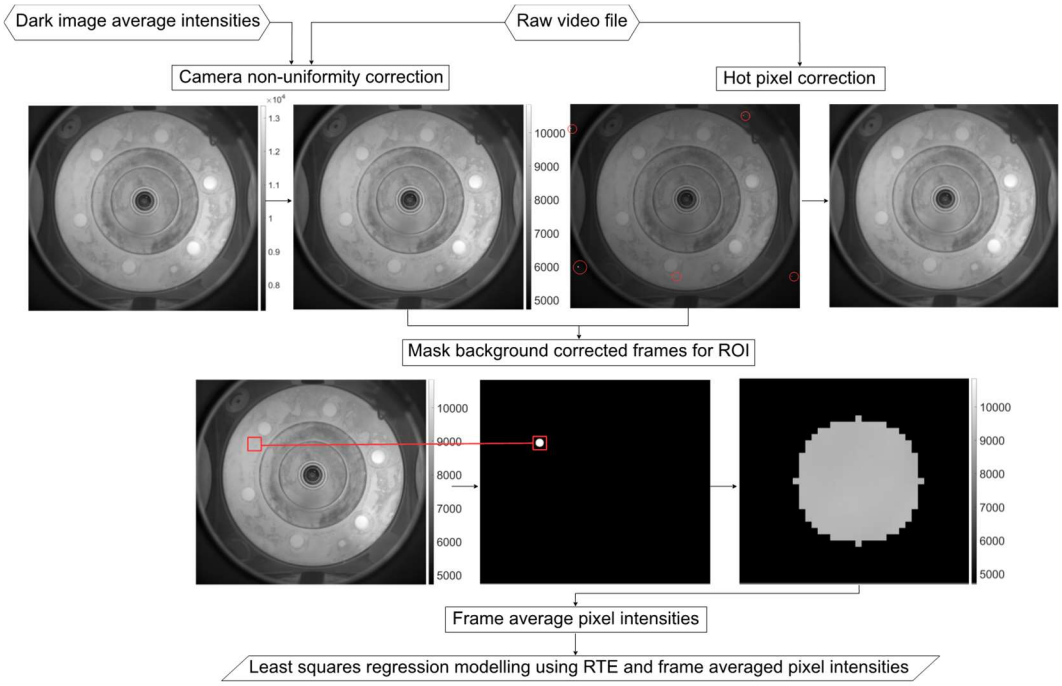

Figure 4. Image processing methodology flow chart for correcting raw IR video frames, masking procedure with ROI, averaging pixel intensities in ROI, and least squares model fitting with RTE equation.

3. Results and discussion

3.1 Effect of superheat on CO_2 removal and absorption capacity

The RTE model fitting results with experimental frame average pixel intensities for condition 120TEA120 are shown in Figure 5. All other conditions follow a similar trend (60TEA60, 90TEA60, 120TEA60). As can be seen between data point 2 ('100 % CO_2 "cold"') and 3 ('100 % CO2 "hot"'), there is a rise in pixel intensity. This rise is associated with the gas heating up and stabilising to the heated vessel's temperature, leading to an increase in CO_2 radiation at the observed wavelength 4.2 µm. There is no change in CO_2 concentration during this thermal stabilisation period. A gradual linear rise in pixel intensity is observed with the experimental data over time, which is caused by the reduction of CO_2 content within the vessel. As the number of CO_2 molecules decrease within the chamber, less IR absorption from the gas is occurring and more IR radiation emitted from the heated injector surface is transmitted

through and received by the IR camera. DBI captures of the spray for each nozzle-chamber temperature condition is shown in Figure 6. In Figure 6(A), minimal flash boiling occurs, and the spray angle remains narrow. With increasing solvent temperature, the spray angle widens, spray penetration increases, and the entire structure collapses towards the centre line of the injector, which is most obvious in Figures 6(B) and 6(C). This structural collapse and denser mid-section at high superheat have been observed in another flash boiling spray investigation of similar liquid temperatures [29]. Figure 6(C) displays the spray forming a “tulip” shape with spray tip vortices becoming visible, which are typical signs of flash boiling and is caused by aerodynamic interaction between the solvent spray creating recirculation zones [36].

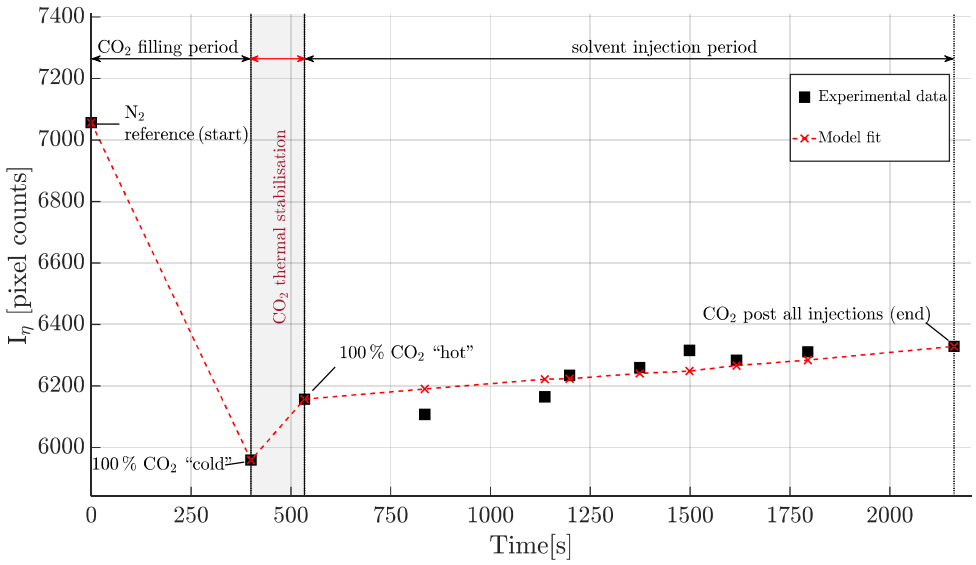

Figure 5. Model fit of I_η as a function of CO_2 density (red data points and dotted line) with experimental data from image processing (black data points). Each experimental data point (1 to 11, starting from the N_2 ref on the left) represents the average intensity of 1 recorded IR video. Process begins on the left when the chamber is filled with N_2 and finishes during the CO_2 purge video. Between data point 2 and 3 (CO_2 thermal stabilisation period), CO_2 concentration remains the same but heats up, leading to a slight increase in radiation.

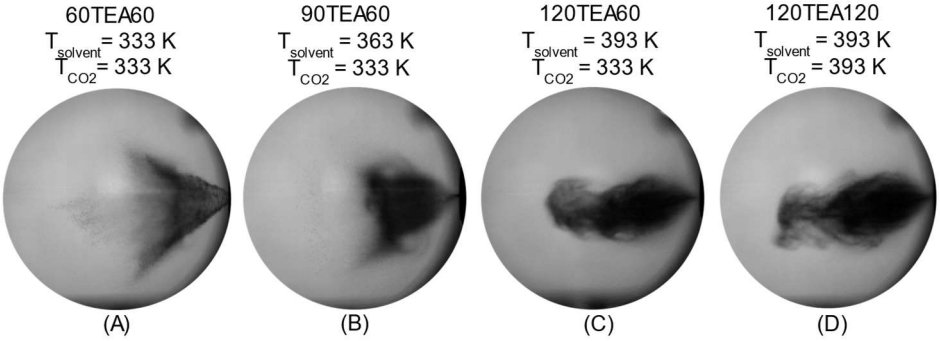

Figure 6. Spray morphology from the POV of the Phantom high-speed camera with image scaling of 0.200 mm/pixel at (A) 333 K solvent temperature and vessel temperature (B) 363 K solvent temperature and 333 K vessel temperature (C) 393 K solvent temperature and 333 K vessel temperature (D) 393 K solvent temperature and vessel temperature.

Absorption capacities were calculated by dividing the number of moles of CO_2 within the chamber by the number of moles of triethanolamine injected. Figure 7 displays calculated absorption capacities (left axis) at each nozzle-chamber temperature condition for this work, alongside available data from the literature on capacities of aqueous triethanolamine blends. Absorption capacity was observed to increase with solvent temperature from 0.093 to 0.16 mol_{CO2} / mol_{amine} from solvent temperature of 333 K to 393 K, which is a 72 % increase. CO_2 temperature had an even greater effect and increased the absorption capacity drastically to 0.46 mol_{CO2} / mol_{amine}. This suggests that an increase in flash boiling superheat improved the CO_2 absorption capabilities of the solvent. However, when looking at the calculated values for absorption capacities in this work (0.093 to 0.45 mol/mol), they generally appear lower than values found in the literature for the same amine at lower temperatures. This is because the solvent blend used in our study was non-aqueous, and water is known to contribute significantly to the physical absorption mechanism for tertiary amines. The *base catalysed hydration* mechanism is the most common theory describing

the chemical reaction between tertiary amine and CO_2. This theory suggests that a hydrogen bond is formed between water and a single molecule of tertiary amine which weakens the hydroxyl group (-OH), thus increasing reactivity and absorbing CO_2 as a bicarbonate [37]:

$$R_3N + H_2O + CO_2 \rightarrow R_3H^+ + HCO_3^- \quad (8)$$

where R_3N is the tertiary amine in general form and HCO_3^- being the final bicarbonate. Both chemical and physical absorption occur for the solvent blend used in this work, but the absence of water inhibited the aqueous physical absorption mechanism (Equation 8). It is important to note in Figure 7 that for the literature data (aqueous TEA), aqueous physical absorption dominates the CO_2 absorption process. In [38] the heats of reaction (enthalpies) were measured and were within the range of 53.4-62.4 [kJ / mol_{CO2}], indicating that a significant exothermic chemical reaction occurred between the aqueous amine and CO_2. The degree to which chemical absorption occurred for aqueous TEA specifically was found to be 39.9 % of the overall absorption time, with the rest being physical absorption [39].

The right axis on Figure 7 is related to the overall drop in concentration over the entire injection period for each nozzle-chamber temperature condition. Drops in CO_2 concentration followed the same trend as absorption capacities, whereby the proportion of CO_2 removed improved steadily (from 5.6 % to 8.9 %) when solvent temperature was increased from 333 K to 393 K. Gas temperature again greatly increased CO_2 removal up to 24 % when at 393 K. This capture performance boost is most likely linked to a corresponding increase in CO_2 diffusion coefficient which is commonly observed at higher temperatures [40, 41]. With a higher diffusion coefficient more CO_2 molecules are able to penetrate and fully saturate the liquid droplets. This explains how even though the flash boiled spray structure between condition 120TEA60 and 120TEA120 are very similar, capture performance is much higher for 120TEA120 due to more CO_2 molecules diffusing and saturating each droplet.

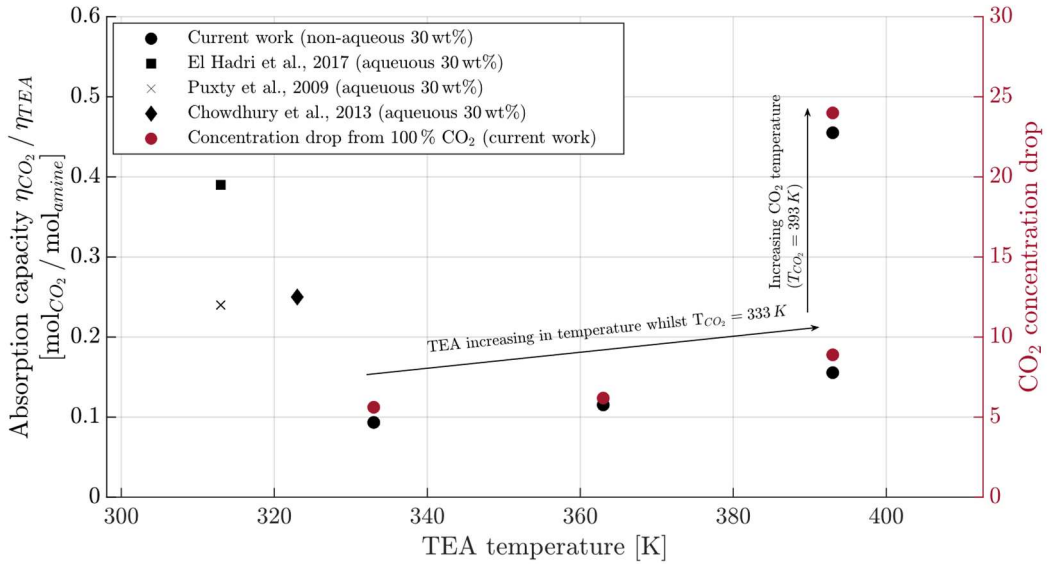

Figure 7. Absorption capacity calculated at each nozzle-chamber temperature condition. All circular data points are related to the work carried out in this investigation. Other shapes indicate absorption capacities of triethanolamine blends from the literature. Red data points are related to the red y axis on the right side.

Conclusions

The effects of flash boiling atomised sprays with varying degrees of superheat for CO_2 removal was experimentally investigated in-situ using an IR optical approach. Superheat was achieved through heating the solvent blend to temperatures 333, 363, 393 K and gas temperatures from 333 K to 393 K. The DBI technique successfully captured temporal spray characteristics and verified the occurrence of flash boiling. Absorption capacities and CO_2 drops were computed for each test condition based on a radiative heat transfer model fitted to the optical experimental data. Although the physical absorption mechanism was inhibited due to a non-aqueous solvent blend, CO_2 removal still occurred at a rate comparable to more energy intensive aqueous solvents. The effectiveness of increasing superheat for CO_2 absorbing flash boiling sprays was also demonstrated for the first time.

The main conclusions can be summarised as follows:

1) Increasing superheat degree through increased solvent temperature improved overall CO_2 removal (up to 8.8 %) and raised the absorption capacity of the solvent blend by 72 % when compared to the lowest nozzle-chamber temperature condition (0.093 to 0.156 mol/mol).

2) Further increasing the gas temperature, coupled with high solvent temperatures, greatly improved the overall CO_2 removal (to 24 %) and absorption capacity (0.45 mol/mol).

Acknowledgements

The authors would like to thank Kyra Schmidt at Sandia National Laboratories for her dedicated support of the Spray Laboratory. The optical measurements were performed at Sandia Nat. Labs in Livermore, CA. Sandia is a multi-mission laboratory managed and operated by National Technology and Engineering Solutions of Sandia, LLC., a wholly owned subsidiary of Honeywell International, Inc., for the U.S. Department of Energy's National Nuclear Security Administration under contract DE-NA000352. This work was funded and supported by the Doctoral Training Alliance (Future Societies).

Nomenclature

I_η	Transmitted intensity [pixel counts]
$I_{\eta,0}$	Incident intensity [pixel counts]
$I_{b\eta}$	Blackbody intensity of medium [pixel counts]
s	Path length [m]
κ_η	Linear absorption coefficient of medium [m^{-1}]
$\kappa_{\rho\eta}$	Mass absorption coefficient [m^2 kg^{-1}]
ρ_{CO_2}	Density of CO_2 [kg m^{-3}]
τ_η	Optical thickness [-]
A	Absorption constant for the optics in the setup (sapphire, lens, filter) [-]

References

[1] Ritchie, H., Roser, M., Rosado, P., 2020, "CO_2 and Greenhouse Gas Emissions" [Online]. Available: https://ourworldindata.org/CO_2-and-greenhouse-gas-emissions [Accessed:19th May 2023]

[2] United Nations Climate Change, 2015, 'The Paris Agreement' [Online]. Available: https://unfccc.int/process-and-meetings/the-paris-agreement [Accessed: 18th May 2023].

[3] Department for Energy Security and Net Zero, Department for Business, Energy & Industrial Strategy, and The Rt Hon Boris Johnson MP, 2020, "The Ten Point Plan for a Green Industrial Revolution" [Online]. Available at: https://www.gov.uk/government/publications/the-ten-point-plan-for-a-green-industrial-revolution#full-publication-update-history [Accessed: 19th May 2023]

[4] Environment Agency, 2021, 'Post-combustion carbon dioxide capture: best available techniques (BAT)' [Online]. Available:https://www.gov.uk/guidance/post-combustion-carbon-dioxide-capture-best-available-techniques-bat#full-publication-update-history [Accessed: 18th Oct 2023].

[5] IECM (Integrated Environmental Control Model Team), 2018, 'Amine-based post-combustion CO_2 capture [Online]. Available: Carnegie Mellon University (cmu.edu) [Accessed: 18th Oct 2023].

[6] Biliyok, C., Lawal, A., Wang, M., and Seibert, F, "2012, Dynamic modelling, validation and analysis of post-combustion chemical absorption CO_2 capture plant", International Journal of Greenhouse Gas Control, 9, pp. 428-445. DOI: 10/f36f4v

[7] Adeosun, A., and Abu-Zahra, M.R., 2013, "Evaluation of amine-blend solvent systems for CO_2 post-combustion capture applications", Energy procedia, 37, pp. 211-218. DOI: 10/j98x

[8] Rochelle, G.T., "Amine scrubbing for CO_2 capture", 2009, Science 325, no. 5948, pp. 1652-1654. DOI: 10/c6snc8

[9] Puxty, G., Rowland, R., Allport, A., Yang, Q., Bown, M., Burns, R., Maeder, M., and Attalla, M., 2009, "Carbon dioxide post combustion capture: a novel screening study of the carbon dioxide absorption performance of 76 amines", Environmental science & technology 43, no. 16, pp. 6427-6433. DOI: 10/ddxv8z

[10] El Hadri, N., Quang, D.V., Goetheer, E.L., and Abu Zahra, M.R.A., 2017, "Aqueous amine solution characterization for post-combustion CO_2 capture process" Applied Energy, 185, pp. 1433-1449. DOI: 10/gpqwqf

[11] Kohl, A. L., and Nielsen, R., 1997, "Gas purification", Elsevier

[12] Kuntz, J., and Adisorn, A., 2009, "Mass-transfer efficiency of a spray column for CO_2 capture by MEA", Energy Procedia 1, 1, pp. 205-209. DOI: 10/dsg23d

[13] Seyboth, O., Simone, Z., Barna, H., and Scheffknecht, G., 2014, "Development of a spray scrubbing process for post combustion CO_2 capture with amine-based solvents", Energy Procedia, 63, pp. 1667-1677. DOI: 10/j98k

[14] Cho, M., Lee, S., Choi, M., and Lee, J.W., 2018, "Novel spray tower for CO_2 capture using uniform spray of monosized absorbent droplets", Industrial & Engineering Chemistry Research, 57, no. 8, pp. 3065-3075. DOI: 10/gc8c2g

[15] Kavoshi, L., Rahimi, A., and Hatamipour, M.S., 2015, "CFD modelling and experimental study of carbon dioxide removal in a lab-scale spray dryer", Chemical Engineering Research and Design, 98, pp. 157-167. DOI: 10/f7g2m4

[16] Ouboukhlik, M., Godard, G., Saengkaew, S., Fournier-Salaün, M.C., Estel, L., and Grehan, G., 2015, "Mass transfer evolution in a reactive spray during carbon dioxide capture." Chemical Engineering & Technology, 38, no. 7, pp. 1154-1164. DOI: 10/f277rb
[17] Michalski, J.A., 2000, "Aerodynamic characteristics of flue gas desulfurization spray towers polydispersity consideration", Industrial & engineering chemistry research, 39, no. 9, pp. 3314-3324 DOI: 10/d4h76x
[18] Seyboth, O., Zimmermann, S., Heidel, B., and Scheffknecht, G., (2014), "Development of a spray scrubbing process for post combustion CO_2 capture with amine-based solvents" Energy Procedia, 63, pp. 1667-1677. DOI: 10/j98k
[19] Xu, Y., Xiaole, C., Zhao, Y., and Jin, J., 2021, "Modelling and analysis of CO_2 capture by aqueous ammonia+ piperazine blended solution in a spray column", Separation and Purification Technology, 267, pp. 118655. DOI: 10/kbhq
[20] Tamhankar, Y., King, B., Whiteley, R., Resetarits, M., Cai, T., and Aichele C., 2014, "Aqueous amine spray absorption and droplet distribution data for CO_2 capture applications", Energy Procedia, 63, pp. 293-300. DOI: 10/kbh2
[21] Ouboukhlik, M., Saengkaew, S., Fournier-Salaün, M.C., Estel, L., and Grehan, G., 2015, "Local measurement of mass transfer in a reactive spray for CO_2 capture" The Canadian Journal of Chemical Engineering, 93, no. 2, pp. 419-426. DOI: 10/f6zj75
[22] Stolaroff, J.K., Keith, D.W., and Lowry, G.V., 2010, "Carbon dioxide capture from atmospheric air using sodium hydroxide spray" Environmental science & technology, 42, no. 8, pp. 2728-2735. DOI: 10/d536hr
[23] Javed, K. H., Mahmud, T., and Purba, E., "The CO_2 capture performance of a high-intensity vortex spray scrubber" Chemical Engineering Journal 162, no. 2, pp. 448-456. DOI: 10/b25s9n
[24] Wu, X., He, M., Yu, Y., Qin, Z., and Zhang, Z., 2017, "Overall mass transfer coefficient of CO_2 absorption in a diameter-varying spray tower", Energy Procedia, 114, pp. 1665-1670. DOI: 10/kbhx
[25] She, J., 2010, "Experimental study on improvement of diesel combustion and emissions using flash boiling injection", SAE Technical Paper, No. 2010-01-0341 DOI: 10/fbvrzt
[26] Senda, J., Wada, Y., Kawano, D., and Fujimoto., H., 2008, "Improvement of combustion and emissions in diesel engines by means of enhanced mixture formation based on flash boiling of mixed fuel", International Journal of Engine Research, 9, no. 1,pp. 15-27.
[27] Reitz, R.D., 1990, "A photographic study of flash-boiling atomization", Aerosol Science and Technology, 12, no. 3, pp. 561-569. DOI: 10/fp6xfb
[28] Shen, S., Jia, M., Wang, T., Lü, Q., and Sun, K., 2016, "Measurement of the droplets sizes of a flash boiling spray using an improved extended glare point velocimetry and sizing", Experiments in Fluids, 57, pp. 1-16. DOI: 10/f8mw68
[29] Zeng, W., Xu, M., Zhang, G., Zhang, Y., and Cleary., D.J., 2012, "Atomization and vaporization for flash-boiling multi-hole sprays with alcohol fuels", Fuel, 95, pp. 287-297. DOI: 10/dtp2fj
[31] Modest, M.F., and Mazumder, S., 2021, "Radiative heat transfer". Academic press.
[32] Oshina, I., Spigulis, J., 2021, "Beer-Lambert law for optical tissue diagnostics: current state of the art and the main limitations", J Biomed Opt, 26, no. 10 DOI: 10/gn63sn
[33] Bernhardsen, I.M., and Knuutila, H.K., 2017, "A review of potential amine solvents for CO_2 absorption process: Absorption capacity, cyclic capacity and pKa", International Journal of Greenhouse Gas Control, 61, pp. 27-48 DOI: 10/f98rqt
[34] Vega, F., Sanna, A., Navarrete, B., Mercedes, M.M., and Cortés, V.J., 2014, "Degradation of amine-based solvents in CO_2 capture process by chemical absorption", Greenhouse Gases: Science and Technology, 4, no. 6, pp. 707-733. DOI: 10/f6rzm6
[35] Luis, P., 2016, "Use of monoethanolamine (MEA) for CO_2 capture in a global scenario: Consequences and alternatives", Desalination, 380, pp. 93-99 DOI: 10/f78xmc
[36] Mojtabi, M., Chadwick, N., Wigley, G., and Helie, J., 2008, "The effect of flash boiling on break up and atomization in GDI sprays" In Proceedings of the 22nd European Conference on Liquid Atomization and Spray Systems, ILASS Europe, Como Lake, Italy, pp. 08-10
[37] Donaldson, T.L., and Nguyen, Y.N., 1980, "Carbon dioxide reaction kinetics and transport in aqueous amine membranes", Industrial & Engineering Chemistry Fundamentals, 19, no. 3, pp. 260-266 DOI: 10/dh7g2h
[38] Chowdhury, F.A., Yamada, H., Higashii, T., Goto, K. and Onoda, M., 2013, "CO_2 capture by tertiary amine absorbents: a performance comparison study", Industrial & engineering chemistry research, 52, no. 24, pp. 8323-8331 DOI: 10/gpqxcg
[39] Han, S.J., and Wee, J.H., 2022, "The Ratio of Chemical and Physical CO2 Absorption Capacity in Triethanolamine and Methyl-diethanolamine Solution Systems", Energy & Fuels 36, no. 11, pp. 5805-5815. DOI: 10/kcq8
[40] Ahmadi, H., Jamialahmadi, M., Soulgani, B.S., Dinarvand, N., and Sharafi, M.S., 2020, "Experimental study and modelling on diffusion coefficient of CO_2 in water", Fluid Phase Equilibria, 523, 112584 DOI: 10/gjpz7n
[41] Versteeg, G. F., Van Dijck, L.A.J., and van Swaaij, W.P.M., 1996, "On the kinetics between CO_2 and alkanolamines both in aqueous and non-aqueous solutions. An overview." Chemical Engineering Communications 144, no. 1, pp. 113-158. DOI: 10/frfs57